CSIRO PUBLISHING

Aust. J. Chem. **2014**, *67*, 192–205
http://dx.doi.org/10.1071/CH13194

Full Paper

A Series of Imidazolyl-Containing Bisphosphonates with Abundant Hydrogen-Bonding Interactions: Syntheses, Structures, and Bone-Binding Affinity

Ling Qiu,[A] *Jianguo Lin,*[A,B] *Liqing Wang,*[A] *Wen Cheng,*[A] *Yang Cao,*[A] *Xuewen Liu,*[A] *and Shineng Luo*[A]

[A]Key Laboratory of Nuclear Medicine, Ministry of Health, Jiangsu Key Laboratory of Molecular Nuclear Medicine, Jiangsu Institute of Nuclear Medicine, Wuxi 214063, China.
[B]Corresponding author. Email: linjianguo@jsinm.org

A series of novel bisphosphonates (BPs) were designed and synthesised as longer-chain analogues of the clinically widely used BP–zoledronate (ZL). They were characterised by mass spectrometry, infrared spectroscopy, NMR spectroscopy, and single-crystal X-ray diffraction. All the crystals are zwitterions with one of the phosphonate oxygen atoms deprotonated and the hydrogen atom transferred to the nitrogen of the imidazole ring. A lot of strong hydrogen bonds are observed among the phosphonate oxygens, hydroxy groups, and protonated nitrogen atoms. An accurate, precise, and robust method was developed to determine the bone binding affinities of BPs based on high performance liquid chromatography. The results show that these five BPs have a strong affinity for hydroxyapatite and the binding capacity decreases when the substituted alkyl groups increase in size.

Manuscript received: 22 April 2013.
Manuscript accepted: 3 September 2013.
Published online: 2 October 2013.

Introduction

Bisphosphonates (BPs), synthetic analogues of pyrophosphate (PP), contain a stable backbone structure of P–C–P which is resistant to enzymatic hydrolysis. They exhibit a high affinity for calcified matrices, such as hydroxyapatite (HA) in bone.[1] Therefore, they are commonly used to inhibit the mineralization of soft tissues and also as a therapy for bone-formation and resorption disorders, e.g. in osteoporosis, Paget's disease, hypercalcemia of malignancy, and bone metastases of several cancers.[2] The BPs adsorb on the bone mineral by forming metal complexes with calcium, and their complexation properties are an important aspect for gaining an understanding of their mechanism of action. On the other hand, the high binding affinities of BPs for bone are of crucial biological significance since they can influence several important activities of these compounds, including uptake and retention by the skeleton, distribution and diffusion of the drug within bone, as well as the release and potential recycling of the drug and cellular functions within bone.[3] The mineral-binding affinity may also affect the appropriate dosing interval and the persistence of effect after discontinuation of medication when BPs are used clinically to treat disorders of bone resorption.[4] Therefore, it is of great importance to design and screen novel BPs with superior mineral-binding affinity.

The structure activities and bone affinities of BPs are directly associated with the substituents (R_1 and R_2) connected both to the middle carbon and to the phosphorus atoms (see Scheme 1).[5,6] In particular, the number of donor atoms in the ligand and their connections with the metal atoms affect the bone affinity significantly. For example, the bone affinity of risedronate (**G**) and etidronate (**C**) is much greater than that of clodronate (**D**) owing to their tridentate adsorption versus the bidentate adsorption of clodronate on the bone mineral surface.[7] That is, a hydroxy group at the R_1 position confers high affinity binding to the mineral. Varying the R_2 substituent can result in differences in the antiresorptive potency of several orders of magnitude, since it is the essential determinant of antiresorptive potency.[8] The most potent antiresorptive BPs include those containing a heteroaromatic moiety with at least one nitrogen atom, such as risedronate (**G**) and zoledronate (ZL, **H**). The enhancement in the antiresorptive potency resulting from different R_2 groups also appears to be linked to the bone-binding ability and biochemical activity of these drugs.[7–9] For example, ZL, containing two nitrogen atoms within a heteroaromatic ring, is at least 100 times more potent than pamidronate (**E**) and at least 1000 times more potent than etidronate (**C**).[10] The structure of the carbon chain attached to the geminal BPs also influences their biological activities. For example, from pamidronate (**E**) to alendronate (**F**) with the carbon chain increasing from 2 to 3, the potency increases 10 times.[11] In addition, two phosphonate groups in the BPs of clinical interest also have a dual function, which are required both for binding to bone mineral and for cell-mediated antiresorptive activity. Modifications to one or both phosphonate groups can dramatically reduce the affinity for bone mineral[7] and the biological potency of the BP.[6]

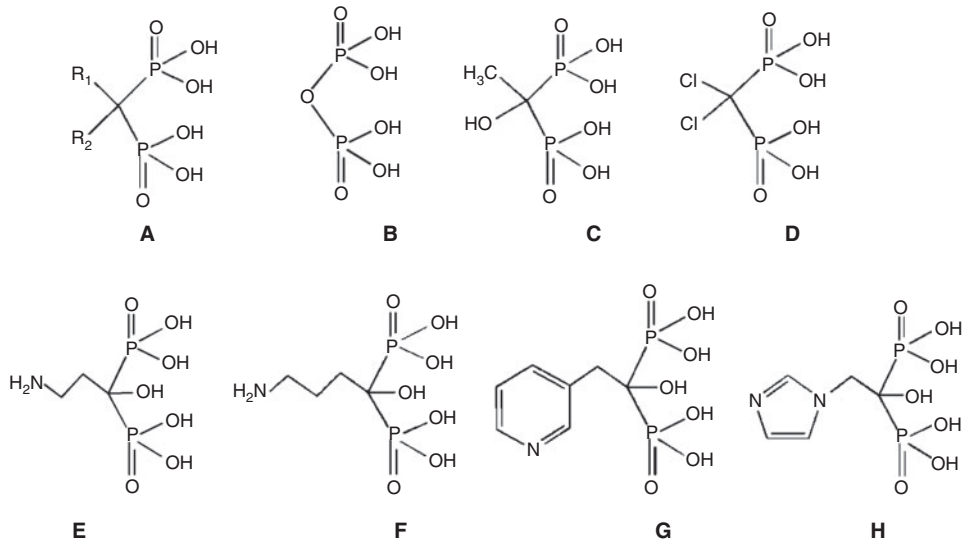

Scheme 1. Generic structure of bisphosphonates (BPs) (**A**) and structures of common BP drugs (all presented in acid form) compared with PP (**B**), etidronate (**C**), clodronate (**D**), pamidronate (**E**), alendronate (**F**), risedronate (**G**), and zoledronate (**H**).

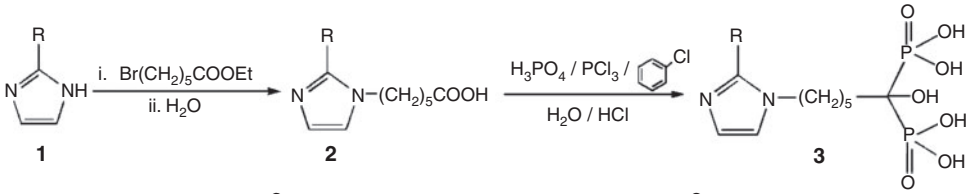

Scheme 2. Syntheses of 1-hydroxy-6-(1*H*-imidazol-1-yl)hexane-1,1-bisphosphonic acid (IHDP, **3a**), 1-hydroxy-6-(2-methyl-1*H*-imidazol-1-yl)hexane-1,1-bisphosphonic acid (MIHDP, **3b**), 1-hydroxy-6-(2-ethyl-1*H*-imidazol-1-yl)hexane-1,1-bisphosphonic acid (EIHDP, **3c**), 1-hydroxy-6-(2-propyl-1*H*-imidazol-1-yl)hexane-1,1-bisphosphonic acid (PIHDP, **3d**), and 1-hydroxy-6-(2-butyl-1*H*-imidazol-1-yl)hexane-1,1-bisphosphonic acid (BIHDP, **3e**).

To date, a large number of BPs have been prepared and investigated.[12] We have also been involved for several years in the synthesis and biological evaluation of imidazolyl-containing BPs to develop novel agents for the diagnosis and therapy of bone diseases.[13] In a continuing effort to find novel BPs with better mineral-binding affinity, in the present work a series of imidazolyl-containing BPs were designed and synthesised (Scheme 2). These compounds can be viewed as longer-chain analogues of ZL, where the imidazolyl with different alkyl groups substituted at the 2-position is linked to the geminal BP unit by a hexylidene group. The synthesis, characterisation, and crystal structures of 1-hydroxy-6-(1*H*-imidazol-1-yl)hexane-1,1-bisphosphonic acid (IHDP, **3a**), 1-hydroxy-6-(2-methyl-1*H*-imidazol-1-yl)hexane-1,1-bisphosphonic acid (MIHDP, **3b**), 1-hydroxy-6-(2-ethyl-1*H*-imidazol-1-yl)hexane-1,1-bisphosphonic acid (EIHDP, **3c**), 1-hydroxy-6-(2-propyl-1*H*-imidazol-1-yl) hexane-1,1-bisphosphonic acid (PIHDP, **3d**), and 1-hydroxy-6-(2-butyl-1*H*-imidazol-1-yl)hexane-1,1-bisphosphonic acid (BIHDP, **3e**) are reported. In addition, the in-vitro bone-binding affinities of these BPs are measured to understand the effect of the carbon chain length of the alkyl groups on the bone-targeting ability. The structure–activity data elucidated for these compounds may be instructive for the design and synthesis of novel BPs.

Experimental

Materials and Measurements

Reagents and solvents as well as HA were commercially available and used as received. Melting points were measured on a Yanaco MP-500 melting point apparatus (Shimadzu, Japan). Electrospray ionisation mass spectrometry (ESI-MS) was performed using a Waters Platform ZMD4000 LC/MS (Waters, U.S.A). ^{1}H NMR spectra were obtained on a Bruker DRX-500 spectrometer (Bruker, Germany), and the chemical shift values were referenced to the internal tetramethylsilane (TMS). Infrared spectra were recorded on a Tensor 27 IR Fourier Transform spectrophotometer using KBr discs (Bruker, Germany).

A high performance liquid chromatography (HPLC) system was equipped with a Waters 1525 binary HPLC pump and a Waters 2487 dual wavelength absorbance detector (Waters, U.S.A). A reverse phase C_{18} (RP-C_{18}) column (4.6 mm × 250 mm; 10 µm particle size) was used for HPLC analysis (Elite Analytical Instrument Co., Dalian, China). The flow rate was 1.0 mL min^{-1}, and the mobile phase was isocratic with 80 % solvent A (4.0 mmol L^{-1} sodium dihydrogen phosphate and 5.0 mmol L^{-1} tetrabutylammonium bromide aqueous solution) and 20 % solvent B (acetonitrile). These conditions are fit for the

purity determination, standard working curve, and HA-binding assay experiments.

Synthesis of BPs

Five new imidazolyl-containing BPs (**3a**–**e**) were synthesised according to the procedure outlined in Scheme 2.[12a]

General Procedure for Preparing Compound **2**

The raw material **1** (0.10 mol) was dissolved in CH_2Cl_2 (100 mL), followed by adding KOH (8.4 g, 0.15 mol), K_2CO_3 (13.8 g, 0.10 mol), and $(Bu)_4NBr$ (0.7 g, 0.002 mol). A solution of $Br(CH_2)_5COOC_2H_5$ (0.1 mol) was added and the reaction mixture was then refluxed for 20 h. To remove the inorganic salt, the solution was filtered and the filtrate was washed with brine solution. The organic phase was dried and evaporated to give the corresponding ester, which was used without further purification in the subsequent reaction. Aqueous HCl (1.2 mol L^{-1}, 100 mL) was added to the crude ester and the mixture was refluxed for 8 h. The solution was concentrated, and the residue was recrystallised from isopropyl alcohol to give the product **2**.

6-(1H-Imidazole-1-yl)hexanoic Acid (**2a**)

The pale white solid was washed with acetone and recrystallised from isopropyl alcohol to obtain 12.6 g of pure white crystals. Yield: 69.3 %, mp 124–126°C. δ_H (400 MHz, D_2O) 8.65 (s, 1H, IMZ-H), 7.44 (s, 1H, IMZ-H), 7.39 (s, 1H, IMZ-H), 4.18 (t, *J* 7.2, 2H, N–CH_2), 2.30 (t, *J* 7.6, 2H, CH_2COOH), 1.81–1.88 (m, 2H, CH_2), 1.52–1.60 (m, 2H, CH_2), 1.22–1.30 (m, 2H, CH_2). *m*/*z* (ESI) 181 (compound **2a**, [M – H]).

6-(2-Methyl-1H-imidazole-1-yl)hexanoic Acid (**2b**)

The reddish brown sticky liquid was crystallised at −5°C and washed with acetone to afford a pale white powder. Recrystallisation of the pale white powder from isopropyl alcohol gave 16.5 g of fine white crystals. Yield: 78.2 %, mp 131–133°C. δ_H (400 MHz, D_2O) 7.34 (d, *J* 2.0, 1H, IMZ-H), 7.29 (d, *J* 2.4, 1H, IMZ-H), 4.10 (t, *J* 7.2, 2H, N–CH_2), 2.60 (s, 3H, CH_3), 2.38 (t, *J* 7.2, 2H, CH_2COOH), 1.81–1.89 (m, 2H, CH_2), 1.59–1.67 (m, 2H,CH_2), 1.31–1.39 (m, 2H, CH_2). *m*/*z* (ESI) 195 (compound **2b**, [M – H]).

6-(2-Ethyl-1H-imidazole-1-yl)hexanoic Acid (**2c**)

The faint yellow sticky liquid was crystallised at 0°C and washed with acetone to afford 13.1 g of a white powder. Yield: 62.5 %, mp 88–90°C. δ_H (400 MHz, D_2O) 7.35 (d, *J* 2.0, 1H, IMZ-H), 7.32 (d, *J* 2.4, 1H, IMZ-H), 4.12 (t, *J* 7.2, 2H, N–CH_2), 2.95–3.01 (q, 2H, ring-C$H_2$$CH_3$), 2.38 (t, *J* 7.2, 2H, CH_2COOH), 1.82–1.90 (m, 2H, CH_2), 1.60–1.67 (m, 2H, CH_2), 1.32–1.39 (m, 5H, CH_2, CH_3). *m*/*z* (ESI) 209 (compound **2c**, [M – H]).

6-(2-Propyl-1H-imidazole-1-yl)hexanoic Acid (**2d**)

The faint yellow sticky liquid was stirred with acetone at −5°C to afford a white powder. Recrystallisation of the white powder from a mixed solvent of isopropyl alcohol/acetone (1 : 2, v/v) afforded 15.6 g of colourless crystals. Yield: 71.2 %, mp 70–72°C. δ_H (400 MHz, D_2O) 7.36 (d, *J* 2.0, 1H, IMZ-H), 7.32 (d, *J* 2.0, 1H, IMZ-H), 4.12 (t, *J* 7.2, 2H, N–CH_2), 2.94 (t, *J* 7.6, 2H, ring-C$H_2$$CH_2$$CH_3$), 2.38 (t, *J* 7.2, 2H, CH_2COOH), 1.82–1.90 (m, 2H), 1.73–1.82 (m, 2H, CH_2), 1.60–1.67 (m, 2H, CH_2), 1.34–1.39 (m, 2H, CH_2), 0.97 (t, *J* 7.2, 3H, CH3). *m*/*z* (ESI) 223 (compound **2d**, [M – H]).

6-(2-Butyl-1H-imidazole-1-yl)hexanoic Acid (**2e**)

The yellowish-brown sticky liquid was triturated with acetone at 0°C, and the mixture precipitated at −20°C. The precipitate was collected through filtration and washed with ethyl acetate. The crude product was then recrystallised from a mixed solvent of isopropyl alcohol/acetone (1 : 2, v/v) to obtain 17.9 g of colourless crystals. Yield: 75.1 %, mp 51–53°C. δ_H (400 MHz, D_2O) 7.36 (d, *J* 2.0, 1H, IMZ-H), 7.32 (d, *J* 2.0, 1H, IMZ-H), 4.13 (t, *J* 7.2, 2H, N–CH_2), 2.97 (t, *J* 7.6, 2H, ring-C$H_2$$CH_2$$CH_2$$CH_3$), 2.38 (t, *J* 7.2, 2H, CH_2COOH), 1.83–1.90 (m, 2H, CH_2), 1.69–1.77 (m, 2H, CH_2), 1.60–1.67 (m, 2H, CH_2), 1.32–1.43 (m, 4H, 2 × CH_2). *m*/*z* (ESI) 237 (compound **2e**, [M – H]).

General Procedure for Preparing Compound **3**

Compound **2** (0.1 mol) was dissolved in chlorobenzene (60 mL) and heated to 110°C for 30 min. After cooling to room temperature, phosphoric acid (85 %, 15.7 mL) was added slowly, followed by phosphorus trichloride (27.3 mL). The reaction mixture was kept at 120°C for 16 h. The chlorobenzene was decanted, and the yellow residue was redissolved in HCl (9 mol L^{-1}, 50 mL). The mixture was refluxed for 10 h. After cooling, charcoal was added to de-colour the solution. After filtration, the solvent was removed. Finally, the crude product was recrystallised from ethanol to give the white powder product **3**. Recrystallisation of the white powder from water afforded white crystals.

1-Hydroxy-6-(1H-imidazol-1-yl)hexane-1, 1-bisphosphonic Acid (**3a**)

Yield 20.6 g (62.8 %), white crystals. Mp 217–220°C. Anal. Calc. for $C_9H_{18}N_2O_7P_2$: C 32.94, H 5.53, N 8.54. Found: C 33.12, H 3.69, N 8.31 %. δ_H (400 MHz, D_2O) 8.66 (s, 1H, IMZ-H), 7.42 (s, 1H, IMZ-H), 7.37 (s, 1H, IMZ-H), 4.18 (t, *J* 6.8, 2H, N–CH_2), 1.81–1.93 (m, 4H, N–CH_2CH_2, CH_2–C–OH), 1.52–1.60 (m, 2H, CH_2), 1.22–1.30 (m, 2H, CH_2). δ_C (100 MHz, D_2O) 140.32 (s, N=C–N), 129.70 (s, C-ring), 122.57 (s, C-ring), 78.80 (t, P–C–P), 49.20 (s, N–CH_2), 38.25 (s, N–CH_2**C**H_2), 32.42 (s, **C**H_2–C–OH), 29.18 (s, CH_2), 25.90 (s, CH_2). ν_{max} (KBr)/cm^{-1} 3396(s, br), 3162(s), 3126(s), 2951 (s), 2860(s), 2389(w, br),1580(m), 1547(w), 1464(m), 1403(w), 1248(m), 1151(s), 1073(v), 989(w), 949(s), 911(m), 767(m), 471(m). *m*/*z* (ESI) 327 (compound **3a**, [M – H]).

1-Hydroxy-6-(2-methyl-1H-imidazol-1-yl)hexane-1, 1-bisphosphonic Acid (**3b**)

Yield 14.6 g (42.7 %), white crystals. Mp 214–216°C. Anal. Calc. for $C_{10}H_{20}N_2O_7P_2$: C 35.10, H 5.89, N 8.19. Found: C 34.87, H 6.05, N 8.08 %. δ_H (400 MHz, D_2O) 7.28 (s, 1H, IMZ-H), 7.20 (s, 1H, IMZ-H), 4.03 (t, *J* 7.2, 2H, N–CH_2), 2.53 (s, 3H, CH_3), 1.86–1.94 (m, 2H, CH_2), 1.76–1.83 (m, 2H, CH_2), 1.52–1.60 (m, 2H, CH_2), 1.24–1.32 (m, 2H, CH_2). δ_C (100 MHz, D_2O) 148.05 (s, N=C–N), 127.12 (s, C-ring), 122.14 (s, C-ring), 78.42 (t, P–C–P), 47.81 (s, N–CH_2), 37.81 (s, CH_3), 31.56 (s, N–CH_2**C**H_2), 28.75 (s, **C**H_2–C–OH), 25.59 (s, CH_2), 13.45 (s, CH_2). ν_{max} (KBr)/cm^{-1} 3279(s, br), 3163(s), 2928(s), 2387 (w, br), 2290(w, br), 1609(m), 1530(w), 1450(w), 1392(w), 1279(w), 1130(m), 1106(m), 1051(s), 1019(s), 970(s), 947(m), 918(m), 759(m), 519(m). *m*/*z* (ESI) 341 (compound **3b**, [M – H]).

Table 1. Crystallographic data and structure refinement for 3a–e

Parameter	3a	3b	3c	3d	3e
Formula	$C_9H_{18}N_2O_7P_2$	$C_{10}H_{22}N_2O_8P_2$	$C_{11}H_{22}N_2O_7P_2$	$C_{12}H_{24}N_2O_7P_2$	$C_{13}H_{26}N_2O_7P_2$
M_w	328.19	360.240	356.25	370.27	384.30
Crystal system	Monoclinic	Monoclinic	Monoclinic	Monoclinic	Orthorhombic
Space group	$P2_1/n$	$P2_1/n$	$P2_1/n$	$P2_1/n$	$Pbca$
T [K]	153(2)	153(2)	153(2)	153(2)	153(2)
a [Å]	9.367(3)	10.296(3)	11.094(4)	9.160(3)	10.3055(17)
b [Å]	7.729(2)	8.906(3)	10.369(3)	20.090(6)	16.810(3)
c [Å]	18.973(6)	16.974(5)	14.078(5)	10.073(3)	20.146(3)
β [deg.]	99.455(4)	98.689(4)	96.614(3)	115.801(2)	90.00
V [Å^3]	1355.0(7)	1538.6(8)	1608.6(10)	1669.0(9)	3490.1(10)
Z	4	4	4	4	8
μ [mm^{-1}]	0.355	0.324	0.305	0.297	0.287
Reflns collected	11630	12817	15866	16692	24620
Unique reflns.	3910	4089	4699	4870	4684
Obs. Reflns. [$I > 2\sigma(I)$]	3209	3603	3899	3915	4167
R_{int}	0.0367	0.0326	0.0308	0.0464	0.0545
R_1 [$I > 2\sigma(I)$][A]	0.0382	0.0526	0.0368	0.0417	0.0618
wR_2 [$I > 2\sigma(I)$][B]	0.1021	0.1184	0.0902	0.0970	0.1412
Goodness-of-fit	0.999	0.999	0.999	1.004	1.000

[A] $R_1 = \Sigma||F_o| - |F_c||/\Sigma|F_o|$. [B] $wR_2 = \{\Sigma[w(F_o^2 - F_c^2)^2]/\Sigma[w(F_o^2)^2]\}^{1/2}$.

*1-Hydroxy-6-(2-ethyl-1*H*-imidazol-1-yl)hexane-1, 1-bisphosphonic Acid (**3c**)*

Yeild 14.0 g (39.9 %), white crystals. Mp 203–205°C. Anal. Calc. for $C_{11}H_{22}N_2O_7P_2$: C 37.09, H 6.22, N 7.86. Found: C 36.91, H 6.50, N 7.75 %. δ_H (400 MHz, D_2O) 7.29 (d, 1H, IMZ-H), 7.23 (d, 1H, IMZ-H), 4.04 (t, *J* 7.2, 2H, N–CH_2), 2.91 (q, 2H, C$H_2$$CH_3$), 1.85–1.94 (m, 2H, CH_2), 1.76–1.84 (m, 2H, CH_2), 1.52–1.60 (m, 2H, CH_2), 1.25–1.32 (m, 5H, –C$H_2$$CH_2$$CH_2$–C–OH, CH_3). δ_C (100 MHz, D_2O) 153.32 (s, N=C–N), 128.03 (s, C-ring), 123.02 (s, C-ring), 79.30 (t, P–C–P), 48.36 (s, N–CH_2), 38.62 (s, ring-CH_2), 32.75 (s, N–CH_2**C**H_2), 29.95 (s, **C**H_2–C–OH), 26.53 (s, CH_2), 21.74 (s, CH_2), 13.93(s, CH_3). ν_{max} (KBr)/cm^{-1} 3387(s, br), 3138(s), 2941(s), 2394(w, br), 1601(m), 1523(w), 1467(w), 1403(w), 1227(w), 1168(m), 1122(s), 993(s), 921(m), 771(w), 459(m). *m*/*z* (ESI) 355 (compound **3c**, [M – H]).

*1-Hydroxy-6-(2-propyl-1*H*-imidazol-1-yl)hexane-1, 1-bisphosphonic Acid (**3d**)*

Yield 22.4 g (40.5 %), white crystals. Mp 206–208°C. Anal. Calc. for $C_{12}H_{24}N_2O_7P_2$: C 38.92, H 6.53, N 7.57. Found: C 38.67, H 6.74, N 7.36 %. δ_H (400 MHz, D_2O) 7.38 (d, *J* 2.0, 1H, IMZ-H), 7.32 (d, *J* 2.0, 1H, IMZ-H), 4.13 (t, *J* 7.2, 2H, N–CH_2), 2.95 (t, *J* 7.6, 2H, C$H_2$$CH_2$$CH_3$), 1.94–2.02 (m, 2H, CH_2), 1.84–1.92 (m, 2H, CH_2), 1.73–1.83 (m, 2H, CH_2), 1.60–1.68 (m, 2H, CH_2), 1.33–1.40 (m, 2H, CH_2), 0.97 (t, *J* 7.2, 3H, CH_3). δ_C (100 MHz, D_2O) 152.16 (s, N=C–N), 128.16 (s, C-ring), 123.15 (s, C-ring), 79.44 (t, P–C–P), 48.49 (s, N–CH_2), 38.84 (s, ring-CH_2), 33.20 (s, N–CH_2**C**H_2), 30.40 (s, **C**H_2–C–OH), 29.93 (s, CH_2), 26.63 (s, CH_2), 23.49(s, CH_2), 15.73(s, CH_3). ν_{max} (KBr)/cm^{-1} 3397(s, br), 3120(s), 2960(s), 2939(s), 2396(w, br), 2289(w, br), 1602(m), 1523(w), 1469(w), 1404(w), 1234(m), 1126(s), 1106(s), 1062(s), 989(s), 924(s), 900 (m), 772(w), 477(m). *m*/*z* (ESI) 369 (compound **3d**, [M – H]).

*1-Hydroxy-6-(2-butyl-1*H*-imidazol-1-yl)hexane-1, 1-bisphosphonic Acid (**3e**)*

Yields 16.5 g (43.0 %), white powder. Mp 191–194°C. Anal. Calc. for $C_{13}H_{26}N_2O_7P_2$: C 40.63, H 6.82, N 7.29. Found: C 40.37, H 7.06, N 7.15 %. δ_H (400 MHz, D_2O) 7.30 (d, *J* 2.0, 1H, IMZ-H), 7.23 (d, *J* 2.0, 1H, IMZ-H), 4.06 (t, *J* 7.2, 2H, N–CH_2), 2.90 (t, *J* 8.0, 2H, C$H_2$$CH_2$$CH_2$$CH_3$), 1.86–1.94 (m, 2H, CH_2), 1.78–1.83 (m, 2H, CH_2), 1.62–1.70 (m, 2H, CH_2), 1.53–1.60 (m, 2H, CH_2), 1.25–1.36 (m, 4H, –C$H_2$$CH_2$$CH_2$–C–OH, –C$H_2$$CH_3$), 0.85 (t, *J* 7.6, 3H, CH_3). δ_C (100 MHz, D_2O) 152.39 (s, N=C–N), 128.64 (s, C-ring), 123.04 (s, C-ring), 79.64 (t, P–C–P), 48.72 (s, N–CH_2), 38.86 (s, ring-CH_2), 32.78 (s, N–CH_2**C**H_2), 31.99 (s, **C**H_2–C–OH), 29.80 (s, CH_2), 27.90 (s, CH_2), 26.54 (s, CH_2), 24.23 (s, CH_2), 15.62 (s, CH_3). ν_{max} (KBr)/cm^{-1} 3411(s, br), 3175(s), 3133(s), 2960(s), 2936 (s), 2388(w, br), 2289(w, br), 1609(m), 1519(w), 1468(w), 1405 (w), 1275(w), 1178(s), 1094(s), 1051(s), 992(s), 942(s), 784(w), 530(m). *m*/*z* (ESI) 383 (compound **3e**, [M – H]).

X-Ray Crystallographic Study

Single crystals of compounds **3a**–**e** in appropriate dimensions were used for structural determinations on a Bruker SMART APEX CCD diffractometer using graphite-monochromatised $Mo_{K\alpha}$ radiation ($\lambda = 0.71073$ Å) at room temperature using the ω-scan technique. Data reductions and absorption corrections were performed with the *SAINT* and *SADABS* software packages, respectively. The structures of all the crystals were solved by direct methods using the *SHELXS-97* program[14] and were further refined by the full-matrix least-squares technique using the *SHELXL-97* program.[15] Anisotropic displacement parameters were refined for all the non-hydrogen atoms except for the disordered atoms. The hydrogen atoms were generated theoretically, allowed to ride on their respective parent atoms, and included in structure factor calculations with assigned isotropic thermal parameters. In the case of compound **3d**, the propyl in the imidazole ring appeared to be disordered over two positions with occupancy factors 0.782 and 0.218, respectively. The crystallographic data and other pertinent information for **3a–e** are summarised in Table 1, while the selected bond lengths and angles are listed in Table 2. More details on the crystallographic studies as well as atom displacement parameters are presented in the .cif files (CCDC 892394–892398), and can be obtained free of charge at www.ccdc.cam.ac.uk/data_request/cif.

Table 2. Selected bond lengths and bond angles for 3a–e

Bonds	3a	3b	3c	3d	3e
Bond lengths [Å]					
P1–C9	1.8465(17)	1.842(2)	1.8494(14)	1.8451(16)	1.842(3)
P2–C9	1.8358(18)	1.832(2)	1.8513(13)	1.8491(17)	1.856(3)
P1–O1	1.5277(13)	1.5517(17)	1.5655(11)	1.5785(13)	1.5514(19)
P1–O2	1.5622(13)	1.5341(17)	1.5433(11)	1.5529(13)	1.562(2)
P1–O3	1.4934(14)	1.4985(17)	1.4916(11)	1.4764(13)	1.486(2)
P2–O4	1.5148(12)	1.5212(16)	1.5055(10)	1.5309(12)	1.511(2)
P2–O5	1.5118(13)	1.5100(16)	1.5103(11)	1.4948(13)	1.514(2)
P2–O6	1.5703(13)	1.5622(17)	1.5663(11)	1.5728(12)	1.5605(19)
C1–C2	1.336(3)	1.347(4)	1.353(2)	1.346(2)	1.346(4)
N1–C1	1.374(2)	1.389(3)	1.383(2)	1.382(2)	1.386(3)
N1–C3	1.334(3)	1.332(3)	1.3366(19)	1.338(2)	1.338(4)
N2–C2	1.363(3)	1.379(3)	1.378(2)	1.377(2)	1.381(4)
N2–C3	1.313(3)	1.325(3)	1.334(2)	1.335(2)	1.332(4)
Bond angles [deg.]					
P1–C9–P2	113.89(9)	114.69(11)	111.82(7)	110.20(8)	109.58(13)
C8–C9–O7	107.31(13)	109.55(16)	104.16(10)	112.73(12)	111.3(2)
O1–P1–O2	110.78(7)	110.05(9)	107.01(7)	104.22(7)	105.43(11)
O1–P1–O3	113.32(8)	112.18(10)	112.45(6)	111.61(7)	113.73(12)
O2–P1–O3	108.60(7)	111.17(10)	110.75(6)	115.38(8)	112.03(11)
C9–P1–O1	110.69(7)	107.39(9)	104.67(6)	104.78(7)	109.20(11)
C9–P1–O2	106.87(8)	108.69(10)	108.05(6)	107.89(7)	105.26(12)
C9–P1–O3	106.28(8)	107.18(10)	113.51(6)	112.15(7)	110.72(11)
O4–P2–O5	114.52(7)	113.60(9)	114.33(6)	113.78(7)	115.31(11)
O4–P2–O6	110.42(7)	110.87(10)	108.25(6)	109.11(7)	110.77(11)
O5–P2–O6	108.02(8)	107.42(9)	111.12(5)	108.77(7)	108.10(11)
C9–P2–O4	111.25(8)	108.04(9)	107.58(6)	107.20(7)	107.11(11)
C9–P2–O5	107.22(7)	111.85(9)	110.12(6)	111.80(7)	109.00(11)
C9–P2–O6	104.89(8)	104.72(9)	104.96(6)	105.86(7)	106.16(11)

HA-Binding Assay

To study the bone targeting efficiency of these BPs, an in vitro HA-binding assay was set up using a HPLC method with the most usual detection system and the simplest chromatography elution conditions. First, all the BPs **3a**–**e** with different concentrations (0.4–6.0 μmol L^{-1}) were determined by HPLC and a standard curve was plotted for each compound from the area integral as a function of concentration (see Fig. S1). The disposition pattern of the standard curve can be described by the following linear equation: $S = kC + b$, where S is the average integral area under HPLC peak of an aliquot of the BP solution, C is the standard concentration of BPs, and k and b are the slope and intercept of the standard curve, respectively.

The adsorption experiments were performed at 37°C in an aqueous medium and incubated for 48 h which is sufficient for reaching the equilibrium of binding. The adsorbed amount of each BP was determined by the difference between the initial compound quantity and that contained in the supernatant solution. The adsorption profile then was obtained as a function of the BP concentration. In detail, aliquots (2 mL) of the BP solution with different concentrations were added to 25 mg of HA in a 10 mL penicillin bottle. After 15 s of treatment in a vortex apparatus, the suspension was maintained in a bascule bath at 37°C. After 48 h of incubation, the mixture was centrifuged at 5000 rpm for 5 min to ensure complete separation of the supernatant from the solid phase. The supernatant was then filtered through a microporous filter (0.22 μm pore size) and an aliquot (10 μL) of the supernatant was removed for the quantification of the BP remaining in the solution by using HPLC analysis. Based on the standard working curves obtained in advance, the amount of BP adsorbed onto HA can be determined by the following formula and expressed as the amount of BP per gram of HA (μmol g^{-1}):

$$\begin{aligned}\text{BP adsorbed}\,(\mu\text{mol g}^{-1}) &= \frac{n_{\text{adsorption}}}{m_{\text{HA}}} = \frac{n_{\text{original}} - n_{\text{supernatant}}}{m_{\text{HA}}} \\ &= \frac{C_0V - C_sV}{m_{\text{HA}}} = \frac{2(C_0k - S + b)}{25k} \times 1000 \\ &= 80\left(C_0 - \frac{S}{k} + \frac{b}{k}\right)\end{aligned}$$

where V is the volume of the solution (2 mL), C_0 is the initial concentration of the bisphosphate solution (μmol mL^{-1}), C_S is the concentration of the supernatant (μmol mL^{-1}), and S is the average area integral under the HPLC peak of an aliquot of the supernatant (10 μL).

Results and Discussion

Synthesis of BPs

Five novel ZL analogues were synthesised by four steps according to a previous method.[12a] In the first step, carboxylic acids **2a**–**e** were prepared through the N-alkylation reaction of 2-alkyl-1*H*-imidazole and $Br(CH_2)_5COOC_2H_5$, which is a heterogeneous reaction. To accelerate the reaction rate and achieve a satisfactory yield, tetrabutyl ammonium bromide (TBAB) was added to the reaction system as a phase transfer catalyst. Compound **2** was then obtained through the hydrolysis with concentrated hydrochloric acid. In the next step, compounds **3a–e** were obtained through the phosphine acidification reaction of the corresponding carboxylic acid **2**. The speed of adding PCl_3

had a critical effect on the yield of the reaction. If the addition is fast, the reaction may be hard to control, and the yield is low. Since adding PCl_3 led to a large amount of precipitate forming immediately, it became more and more difficult to stir. This will result in incomplete conversion from the carboxylic acid to the bisphosphonic acid. Otherwise, the reaction time may be too long. So, a moderate speed of addition ($\sim$0.4 mL min^{-1}) was selected to control the reaction temperature and increase the yield.

On the other hand, crystallisation of the obtained faint yellow or colourless oil was also important but very tedious, as previously described by others.[12a–d] To address this problem, many changes have been made by us and now it is easy to get pure compounds. Under continuous stirring, the residual oil was added slowly to a large amount of ethanol and the crude product precipitated immediately. After 24 h, the suspension was filtered to give a fine white powder, which was very stable at room temperature. In this way, the separation and purification became easier and more efficient. The yield was moderate, even rather low (typically 35–40 %). However, there are a few advantages of this reaction including cheap and easily available reagents as well as simple operation. More importantly, the residual carboxylic acid and chlorobenzene as well as phosphoric acid can be easily separated by dissolving them in the ethanol.

Spectroscopic Characterisation

Compounds **3a**–**e** were fully characterised by melting point, MS, and FT-IR and ^{1}H NMR spectroscopy. From **3a** to **3e** with the substituent at the 2-position of the imidazole ring changing from hydrogen to butyl, the melting point decreases from 220 to 191°C. This may be attributed to the stereo-hindrance effect of the side substituent R, which leads to a more and more loose structure. The molecular ions excited by the ESI method confirmed the proposed molecular formula of all BPs.

The IR spectra of five BPs are similar to each other. All of them show that the typical strong absorption bands of the C=O stretching vibrations in the carboxylic acids **2** disappear and three new characteristic absorption bands occur. The bands in the region of 1126–1279 cm^{-1} are associated with the typical symmetric and asymmetric stretching vibrations of PO_2 from PO_3H^- groups. The absorption bands at 940–1000 cm^{-1} and around 1080 cm^{-1} are attributed to the vibration modes of ν_s(P–OH) and δ(P–OH), respectively, which are due to the deprotonated POH groups in these compounds.[16] In addition, the absorption bands at $\sim$3100 cm^{-1} correspond to the stretching vibrations of the protonated N2.

The ^{1}H NMR spectrum of compound **3a** shows three single peaks in the region of 7.37–8.66 ppm, corresponding to the protons in the aromatic imidazole ring, while those of compounds **3b**–**e** show two doublets ($^3J = 2$ Hz) in the region of 7.20–7.38 ppm. Similar ^{1}H NMR spectra are also observed for the compounds **2a**–**e**. They agree well with the expected chemical structures of all the bisphosphonic acids and carboxylic acids.

In addition, the purity of compounds **3a**–**e** was also checked by HPLC (see Fig. 1). For each compound, only one single peak was observed. This clearly showed the high purity of the compounds. The retention times of compounds **3a**–**e** were 5.95, 6.07, 6.50, 7.40, and 11.05 min, respectively. It is evident that the substituent at the 2-position of the imidazole ring affects the retention behaviour of these BPs. Under the same mobile phase conditions, the retention time was extended as the number of carbon atoms in the substituent increased.[17] Especially for

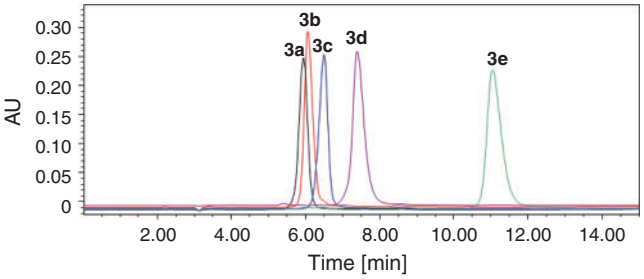

Fig. 1. HPLC analyses of compounds **3a–e**.

compound **3e**, the extension is the most remarkable corresponding to the butyl group which has the maximum number of C atoms within the compounds under investigation (from 5.95 to 11.05 min). This is due to the fact that the bulky lipophilic alkyl group has a significant influence on the polarity of the compound, which changes the retention time accordingly.

Crystal Structures

Single crystals of compounds **3a**–**e** were obtained with a quality good enough for X-ray crystallography analysis. The structures of five compounds have been solved and refined (see Table 1). The single crystal X-ray diffraction studies reveal that compounds **3a**–**d** all crystallise in the monoclinic space group $P2_1/n$ and contain four irreducible molecules per unit cell, while **3e** crystallises in the orthorhombic space group *Pbca* with eight irreducible molecules in the unit cell which is different from other compounds. In addition, although all the crystals are recrystallised from water, only compound **3b** has a water solvent molecule in the crystal structure. In the asymmetric unit of **3b**, there is one lattice water molecule per BP molecule. Compared with other compounds, the additional lattice water molecule in **3b** may increase the donor and acceptor property towards hydrogen bonds and build a more complicated hydrogen-bonded system. In the asymmetric unit of **3d**, there is disorder at the propyl group and only the propyl attached to the imidazole ring with a high occupancy factor (0.782) has been shown. The phenomenon of the propyl side chain is disordered over two sites with different occupancies were also observed in other reported structures.[18]

As anticipated, all the crystals **3a**–**e** are zwitterions, in which one of the phosphonate oxygen atoms is ionised and the hydrogen atom is transferred to the nitrogen atom (N2) of the imidazole ring (see Fig. 2). This behaviour is not an uncommon feature for the nitrogen-containing bisphosphonates (NBPs), as has been observed previously for ZL[19] and other related compounds.[12a-d,20] According to the previous investigation,[12d] the protonated side chains of the NBPs are important for their binding to the farnesyl diphosphate synthase target and they are useful for treating various bone resorption diseases.

Inspection of the bond distances in the protonated imidazole ring shows that there are two classes of C–N bonds in the ring. As illustrated in the diagram for **3a**, the longer bonds (C1–N1 1.374(2) Å, C2–N2 1.363(3) Å) represent essentially single-bond character at C1–N1 and C2–N2 (1.340–1.358Å),[21] while the short ones (C3–N1 1.334(3) Å, C3–N2 1.313(3) Å) imply partial double-bond character between atoms C3 and N1/N2 (1.314 Å).[21] The other double bond in the ring is found at C1–C2. This structure shows an approximately equal charge distribution on the atoms N1 and N2. As the hydrogen at the 2-position of the imidazole ring was substituted by methyl, ethyl, propyl, and butyl groups, i.e. from **3a** to **3e**, a slight increase was

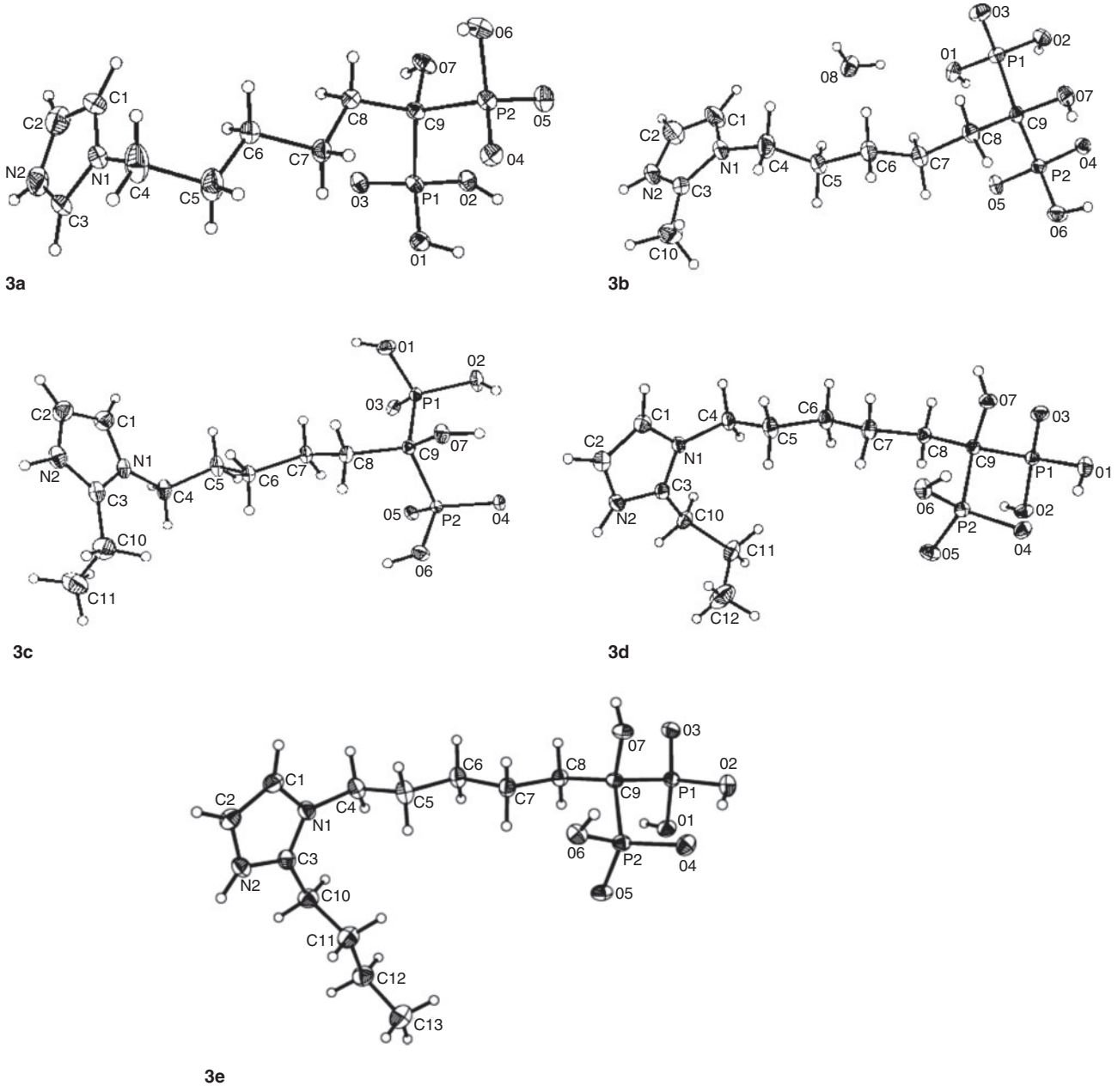

Fig. 2. The asymmetric units of **3a** (1-hydroxy-6-(1*H*-imidazol-1-yl)hexane-1,1-bisphosphonic acid, IHBP), **3b** (1-hydroxy-6-(2-methyl-1*H*-imidazol-1-yl) hexane-1,1-bisphosphonic acid, MIHBP · H_2O), **3c** (1-hydroxy-6-(2-ethyl-1*H*-imidazol-1-yl)hexane-1,1-bisphosphonic acid, EIHBP), **3d** (1-hydroxy-6-(2-propyl-1*H*-imidazol-1-yl)hexane-1,1-bisphosphonic acid, PIHBP), and **3e** (1-hydroxy-6-(2-butyl-1*H*-imidazol-1-yl)hexane-1,1-bisphosphonic acid, BIHBP) with atomic displacement ellipsoids drawn at the 50 % probability level.

observed for all the bond lengths in the imidazole ring, particularly for the bonds N2–C3 and N2–C2 (see Table 2). This mainly stems from the repulsive force between the hydrogen atom on the protonated N2 and the alkyl group introduced at the neighbouring position.

In compounds **3a**–**e**, the relative positions of the two phosphonate groups are nearly eclipsed when viewed along the P–C–P axis, and the chain of atoms O3–P1–C9–P2–O6 form an approximately planar 'W' configuration with a torsion angle of ~2.7°. On two sides of this plane, two pairs of phosphonate oxygen atoms (O1 and O4, O2 and O5), hydroxyl, and methylene groups are equally distributed. Such an arrangement provides a minimum of repulsion among the substituent R_1, R_2, and the phosphonate oxygens.

The geometries of atoms P1 and P2 are all approximately tetrahedral with small deviations induced by different environments of the oxygen atoms O1/O2/O3 and O4/O5/O6. This can be indicated by the bond angles O–P–O and C–P–O given in Table 2. The bond angles of O–P1–O range from 104.22° to 115.38°, while those of O–P2–O lie between 107.42° and 115.31°. The bond angles of C9–P1–O range from 104.67° to 113.51°, while those of C9–P2–O lie between 104.72° and 111.85°. As a whole, the bond angle O4–P2–O5 with a mean value of 114.31° is larger than other O–P–O bond angles with mean value of 110.06°, which is probably attributed to the repulsive interaction between two unprotonated atoms O4 and O5. Similarly, the C–P–O angles involving unprotonated oxygen atoms (O3, O4, and O5) are obviously larger than those

involving protonated oxygen atoms (O1, O2, and O6). In addition, the angle between two phosphonate groups, i.e. P–C–P, decreases slightly on the whole due to the repulsive force between the side chains increasing from **3a** to **3e**. However, they are still close to the observed P–C–P conformation in other BPs.[12d,20]

The P–O bonds in all compounds fall into two distinct classes. One contains the unprotonated oxygen atoms, i.e. P=O or P–O$^-$, which ranges from 1.48 to 1.53 Å in length, suggesting a resonant partial double bond character (1.45–1.50 Å),[21] the other contains the protonated oxygen atoms, i.e. P–OH, which ranges from 1.53 to 1.58 Å in length, representing a single bond character (1.56–1.68 Å).[21] This is in good agreement with previous studies.[12d,20] No significant discrepancy was observed between the double bond (P=O) and single bond (P–O), indicating the importance of resonance effects in these systems. Moreover, the P–O bonds having oxygen atoms involved in strong hydrogen bonds are considerably shorter than those having the oxygen atom involved in weak hydrogen bonds. For example, in **3a** the bond length of P1–O1 is 1.5277 (13) Å, while those of P1–O2 and P2–O6 are 1.5622(13) and 1.5703(13) Å, respectively (see Table 2). It changes in the order of P1–O1 < P1–O2 < P2–O6, consistent with the variation of the corresponding hydrogen bond length O1–H1O···O5^{i} < O2–H2O···O4^{i} < O6–H6O···O4^{ii} (see Table 3, which has listed the hydrogen bond details). The same is true for compounds **3b**–**e**.

Molecules in the crystals **3a**–**d** pack as tetramers while those in **3e** as octamers, which are formed mainly due to the intermolecular hydrogen bonding interactions. The hydrogen bonding scheme for **3a**–**e** consists of O–H···O and N–H···O interactions (Table 3) where the O···O and N···O distances are far less than the sum of the van der Waals radii of 3.04 and 3.07 Å, respectively,[22] which play an important role in stabilising the layered networks of all the crystals. The phosphonate oxygen atoms (O1, O2, and O6) and the hydroxy oxygen atom (O7) as well as the protonated nitrogen atom (N2) of the imidazole ring all serve as the hydrogen bond donors, while the phosphonyl oxygen atoms (O3, O4, and O5) in the neighbouring molecule act as the hydrogen bond receptors. In compound **3a**, dimers are first generated by the symmetrical hydrogen bonds O1–H1···O5 and O2–H2···O4 between two phosphonate groups of two independent molecules, which act as a cyclic motif $R_2^2(8)$determining the formation of two eight-membered rings O4···H2–O2–P1–O1–H1···O5–P2. The dimers are then linked together and continue into a tetramer by another hydrogen bond O6–H6···O4 as a cyclic motif $R_2^2(8)$, leading to the formation of a new kind of eight-membered ring O6–H6···O4–P2–O6–H6···O4–P2. This generates a one-dimensional (1D) chain of dimers running along the *b* direction (Fig. 3a). The cohesion between chains of dimers is further developed by O7 and N2 by cooperative hydrogen bonds with O3, O7–H7O···O3^{iii} and N2–H2N···O3^{iv}, which determines the formation of two-dimensional (2D) layered network and three-dimensional (3D) supramolecular framework, respectively (see Figs 3b and 3c).

In **3b,** extensive hydrogen bonding interactions are also observed among the phosphonate groups, hydroxy groups, and protonated nitrogen atoms. In addition, the lattice water molecule also provides hydrogen bonds between molecules in the tetramer, which not only serves as the hydrogen bond donor but also acts as the hydrogen bond receptor (see Fig. 4). First, the O1–H1O···O4^{ii} and O2–H2O···O5^{ii} hydrogen bonds between neighbouring phosphonate oxygen atoms act as a motif $R_2^2(12)$ and connects the zwitterions of **3b** into dimers. The dimers are then linked together by cooperative hydrogen bonds with the lattice water oxygen atom (O8) through one donor contact O8–H8B···O1 and a receptor contact O6–H6···O8, forming a chain of dimers along the *b* axis (Fig. 4a). The hydrogen bonds from adjacent chains, O8–H8A···O3^{i} and O7–H7O···O3^{iv}, lead to the formation of a 2D layered network, where the lattice water molecule gives further cohesion to this entity (Fig. 4b). Finally, the 2D layers are further stabilised by the hydrogen bonds N2–H2N···O4^{v} and assembled into a 3D supramolecular network (Fig. 4c).

In **3c**, the symmetrical hydrogen bonds O1–H1O···O5^{i} between neighbouring phosphonate groups of two adjacent molecules form a cyclic motif $R_2^2(8)$ and connect the zwitterions of **3c** into dimers. The dimers are then linked together and continue into a 1D zigzag chain along the *b* axis by the hydrogen bonds O6–H6O···O3^{iii} between another two phosphonate oxygens, which also act as a cyclic motif $R_2^2(8)$ (Fig. 5a). The cohesion between chains of dimers is further developed by O2 and O7 by cooperative hydrogen bonds with O4, O2–H2O···O4^{ii} and O7–H7O···O4^{ii}, determining the formation of

Table 3. Geometric description of hydrogen-bonding interactions for 3a–e

Symmetry codes for **3a**: (i) –*x*, 2 –*y*, 1 –*z*; (ii) –*x*, 1 –*y*, 1 –*z*; (iii) 1 –*x*, 2 –*y*, 1 –*z*; (iv) 1.5 –*x*, –0.5 + *y*, 1.5 –*z*. **3b**: (i) 0.5 –*x*, –0.5 + *y*, 1.5 –*z*; (ii) –*x*, 1 –*y*, 1 –*z*; (iii) *x*, 1 + *y*, *z*; (iv) 0.5 –*x*, 0.5 + *y*, 1.5 –*z*; (v) 1 + *x*, –1 + *y*, *z*. **3c**: (i) 0.5 –*x*, 0.5 + *y*, 1.5 –*z*; (ii) –*x*, 1 –*y*, 1 –*z*; (iii) 0.5 –*x*, –0.5 + *y*, 1.5 –*z*; (iv) 1 + *x*, *y*, *z*. **3d**: (i) 1 –*x*, 1 –*y*, 1 –*z*; (ii) 1 –*x*, 1 –*y*, 2 –*z*; (iii) –*x*, 1 –*y*, 1 –*z*; (iv) 1.5 –*x*, –0.5 + *y*, 1.5 –*z*. **3e**: (i) 1 –*x*, 1 –*y*, 1 –*z*; (ii) 0.5 + *x*, 1.5 –*y*, 1 –*z*; (iii) –0.5 + *x*, 1.5 –*y*, 1 –*z*; (iv) 1.5 –*x*, 1 –*y*, 0.5 + *z*.

D–H···A	*d*(D–H) [Å]	*d*(H···A) [Å]	*d*(D···A) [Å]	∠DHA [deg.]
3a				
O1–H1O···O5^{i}	0.8400	1.6300	2.4316(19)	159.100
O2–H2O···O4^{i}	0.8400	1.7700	2.5724(19)	160.400
O6–H6O···O4^{ii}	0.8400	1.7800	2.6152(18)	172.400
O7–H7O···O3^{iii}	0.8400	1.9100	2.6575(18)	147.200
N2–H2N···O3^{iv}	0.86(3)	1.83(3)	2.674(2)	165.0(3)
3b				
O8–H8B···O1	0.836(10)	2.004(11)	2.831(2)	170.0(4)
O8–H8A···O3^{i}	0.835(10)	1.920(15)	2.707(3)	157.0(3)
O1–H1O···O4^{ii}	0.8400	1.6700	2.475(2)	160.900
O2–H2O···O5^{ii}	0.8400	1.6700	2.474(2)	159.600
O6–H6O···O8^{iii}	0.8400	1.7600	2.555(2)	156.600
O7–H7O···O3^{iv}	0.93(5)	1.78(5)	2.702(2)	174.0(5)
N2–H2N···O4^{v}	0.86(4)	2.05(4)	2.839(3)	152.0(4)
3c				
O1–H1O···O5^{i}	0.82(3)	1.74(3)	2.5557(15)	172.0(3)
O2–H2O···O4^{ii}	0.8400	1.6700	2.4814(16)	162.300
O6–H6O···O3^{iii}	0.85(2)	1.72(2)	2.5628(15)	171.0(2)
O7–H7O···O4^{ii}	0.86(2)	1.94(2)	2.7507(16)	156.0(19)
N2–H2N···O5^{iv}	1.02(2)	1.76(2)	2.7434(17)	162.0(2)
3d				
O1–H1O···O4	0.8400	1.9300	2.6964(18)	151.400
O2–H2O···O5^{i}	0.8400	1.6800	2.4978(18)	163.800
O6–H6O···O4^{ii}	0.8400	1.7700	2.5920(18)	165.500
O7–H7O···O3^{iii}	0.8400	1.8600	2.6890(18)	170.900
N2–H2N···O4^{iv}	0.89(2)	1.91(3)	2.782(2)	166.0(2)
3e				
O2–H2O···O4	0.8400	1.7800	2.596(3)	162.000
O1–H1O···O5^{i}	0.8400	1.7500	2.551(3)	160.000
O6–H6O···O3^{ii}	0.8400	1.7400	2.566(3)	167.600
O7–H7O···O4^{iii}	0.8400	2.0200	2.837(3)	165.700
N2–H2N···O5^{iv}	0.88(5)	1.91(5)	2.774(3)	167.0(4)

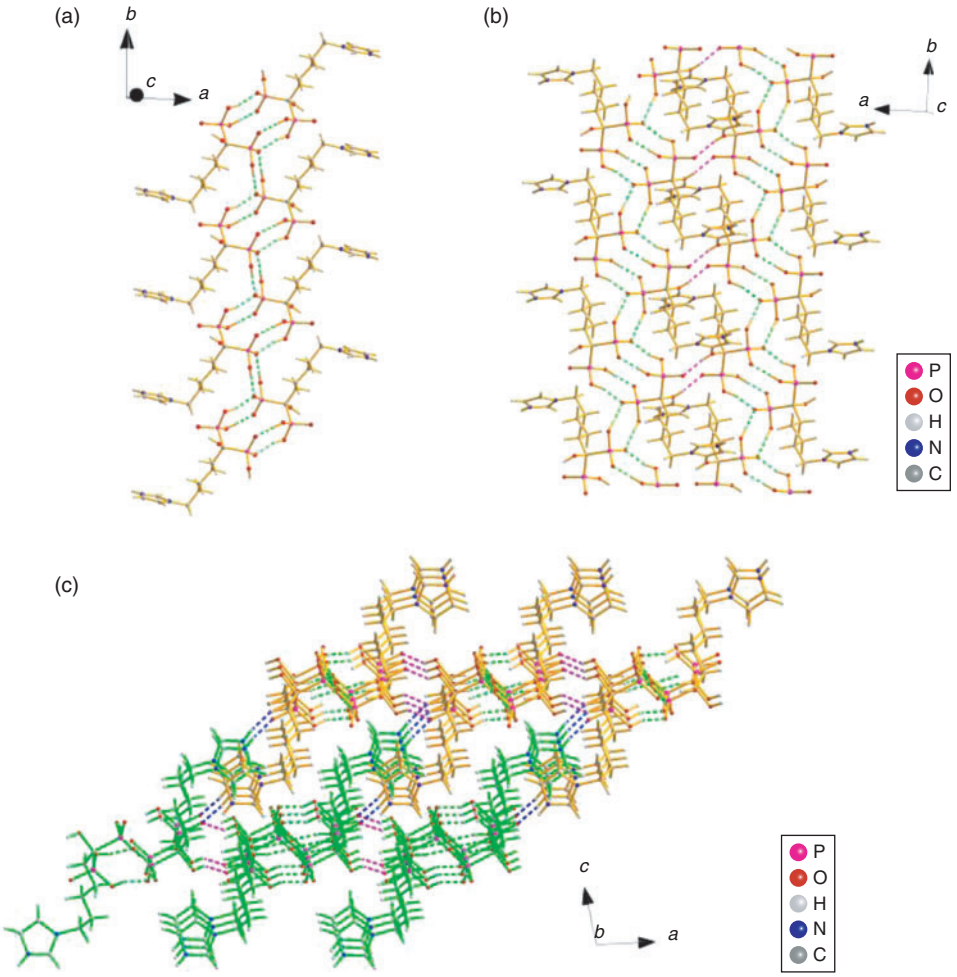

Fig. 3. Perspective view of the supramolecular network of compound **3a** formed by the hydrogen-bonding interactions from 1D (a), 2D (b), to 3D (c). Dashed lines represent hydrogen bonds.

a 2D layered network (Fig. 5b). Finally, a 3D supramolecular network is further assembled by the strong hydrogen bonds between the protonated N2 atoms and phosphonate oxygen atoms (N2–H2N···O5^{iv}, 2.7434(17) Å) (Fig. 5c).

The hydrogen bonding observed in the crystals of **3d** and **3e** are quite similar to each other. The symmetrical hydrogen bonds O2–H2O···O5^{i} (**3d**) and O6–H6O···O3^{ii} (**3e**) between neighbouring phosphonate groups of two adjacent molecules produce a cyclic motif $R_2^2(12)$ and connect the zwitterions of **3d/3e** into dimers respectively. The dimers in **3d** are then further assembled into a 1D zigzag chain along the *c* axis by O6–H6O···O4^{ii} hydrogen bonds which act as a cyclic motif $R_2^2(8)$(Fig. 6a), while those in **3e** are connected by the hydrogen bonds O1–H1O···O5^{i} and also form a 1D zig-zag chain of dimers along the *b* axis (Fig. 7a). Both the 2D layered networks of **3d** and **3e** are formed by the interchain hydrogen bonds between the side hydroxy and the phosphonyl oxygens (**3d**: O7–H7O···O3^{iii}, 2.6890(18) Å; **3e**: O7–H7O···O4^{iii}, 2.837(3) Å), see Figs 6b and 7b. As listed in Table 3, there are also strong N–H···O hydrogen bonding interactions between the protonated N2 atoms and phosphonate oxygen atoms in **3d** and **3e** (N2–H2N···O4^{iv}, 2.782(2) Å and N2–H2N···O5^{iv}, 2.774(3) Å), which further extend the 2D layers into the 3D supramolecular frameworks (Figs 6c and 7c).

The structural parameters deduced from X-ray diffraction show correlations with the chemical and physical data measured for the compounds, such as melting point. For example, the strongest hydrogen bond occurs in **3a**, O1–H1O···O5^{i} (2.4316(19) Å), corresponding to the highest melting point of 217–220°C. It is followed by **3b** with stronger hydrogen bonds (O1–H1O···O4^{ii}, 2.475(2) Å and O2–H2O···O5^{ii}, 2.474(2) Å), corresponding to a higher melting point of 214–216°C. The weakest hydrogen bonding occurs in **3e**, O7–H7O···O4^{iii} (2.837 (3) Å), corresponding to the lowest melting point of 191–194°C, while **3c** and **3d** show an intermediate melting point (203–205 and 206–208°C) due to the intermediate hydrogen bonding (O2–H2O···O4^{ii}, 2.4814(16) Å and O2–H2O···O5^{i}, 2.4978 (18) Å). Here, it should be pointed out that although the weakest hydrogen bond N2–H2N···O4^{v} (2.839(3) Å) in **3b** is slightly longer than the weakest hydrogen bond (O7–H7O···O4^{iii}, 2.837 (3) Å) in **3e**, **3b** has a higher melting point than **3e**. This is because **3b** has more and shorter intermolecular hydrogen bonds than **3e**, which partly contribute to the additional cohesion caused by the lattice water molecules in **3b**. Therefore, the hydrogen bonding in **3b** is more compact than **3e**. Clearly, the melting point dropping from 220 to 191°C indicates the hydrogen-bonded system varying from tight to loose for compounds **3a**–**e**. This mainly originates from the differences in the alkyl group substituted at the neighbouring position of the protonated nitrogen atom, which may cause different stereohindrance effects.

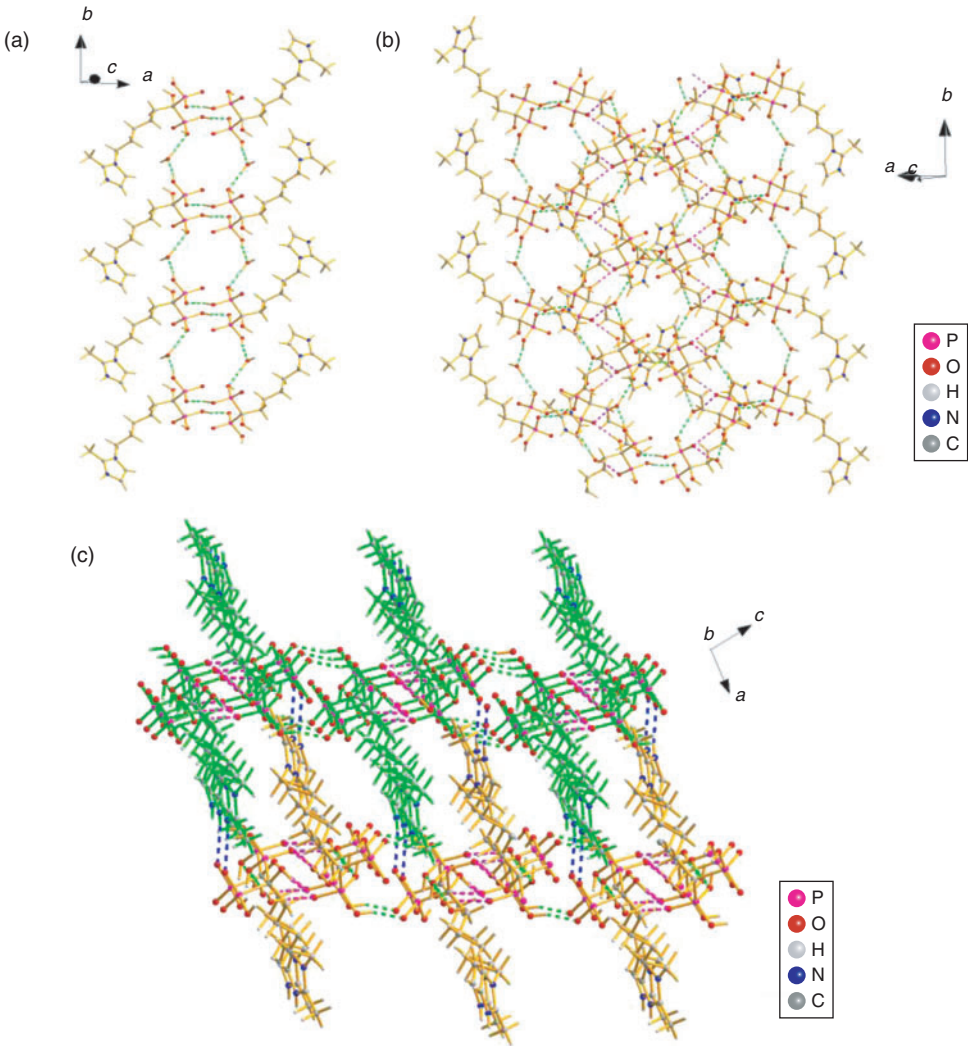

Fig. 4. Perspective view of the supramolecular network of compound **3b** formed by the hydrogen-bonding interactions from 1D (a), 2D (b), to 3D (c). Dashed lines represent hydrogen bonds.

HA-Binding Assay

From the above single-crystal XRD studies, it is known that extensive hydrogen bonding interactions exist among the phosphonate oxygens, hydroxy groups, and protonated nitrogen atoms as well as the lattice water molecules in compounds **3a**–**e**. The existence of such abundant hydrogen bond donors and receptors leads to the concept that these novel BPs can interact strongly with the HA or bone mineral. So, the binding affinity of **3a–e** for HA was investigated.

In the past, several methods have been developed for in vitro assay to measure binding affinities of small molecules to HA, such as X-ray photoelectron spectroscopy (XPS),[23] NMR spectroscopy,[24] fluorescent labelling,[25] and constant composition potentiostatic methods.[7] Also, a method based on fast performance liquid chromatography (FPLC) uses columns of HA, to which BPs and other phosphate-containing compounds can adsorb and be eluted.[26] Even though these methods can qualify binding affinities, a more accurate, precise, and economic method should be developed. In the present work, to quantify the bone targeting efficiency of the BPs **3a–e**, a new method was set up using HPLC which employs the most common detection system and the simplest chromatography elution conditions found in experimental and clinical laboratories. In fact, it provides an accurate, precise, and robust method for quantitative analysis of these bisphosphates using UV detection and isocratic conditions.

Fig. 8 shows the adsorption profiles of **3a**–**e** on HA as function of the concentration of BPs. The plots show that the amount of BP bound to HA increases up to a saturation level with the initial amount of each BP in solution increasing, and the binding characteristic follows the classical Langmuir adsorption isotherm. The results also clearly show that all the BPs studied in the present work have a strong affinity for HA. In their acid forms (pH 2.85), the maximum adsorption amounts of **3a**–**e** are ~158.10, 111.10, 97.33, 91.35, and 83.59 µmol per gram of HA, respectively. So, the binding capacity appears to decrease in the order of **3a** > **3b** > **3c** > **3d** > **3e**. The maximal amount of **3a** bound to HA is much higher (nearly 1.5 to 1.9 fold) than those of **3b**–**e** because of only a small difference in the substituent R_2. As shown in the previous study,[26] when the risedronate was attached to an extra methyl group in the R2 side chain, the two BPs had different retention times (16.16 and 14.41 respectively) indicating the decrease of HA binding affinity. As detected by a constant composition

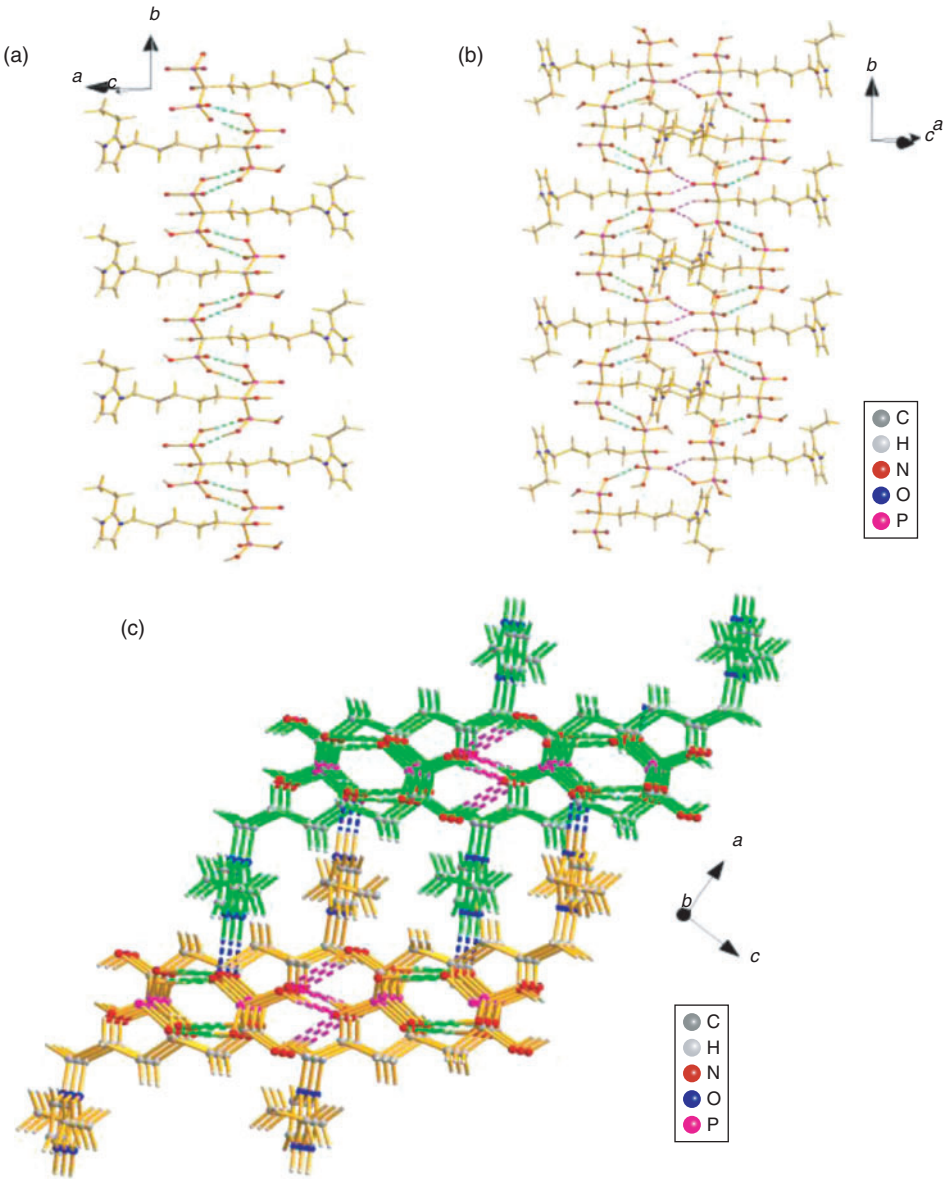

Fig. 5. Perspective view of the supramolecular network of compound **3c** formed by the hydrogen-bonding interactions from 1D (a), 2D (b), to 3D (c). Dashed lines represent hydrogen bonds.

potentiostatic method, Nancollas et al. demonstrated significant differences in the binding affinity of similar BPs to HA and carbonated apatite and established a rank order of ibandronate < alendronate < pamidronate.[7,27,28] So, the results further demonstrate that the nature of the R_2 side chain has a significant influence on the binding affinity although they share a common P–C–P structure and OH at the R_1 side chain. On the other hand, it is known that small differences in the R_2 group lead to substantial changes in the 3D shapes and atomic orientations of the BPs according to the above single-crystal XRD studies. Therefore, it is postulated that the 3D configuration of the imidazolyl-containing BPs and the orientation of the imidazolyl group may play an important role in the mineral binding affinity.[8]

Based on the established interaction model of simpler BPs on HA where the tridentate coordination of the P–C–P 'bone hook' and R_1 (–OH) domains interact with the calcium site,[8] there is the potential of additional interactions between the imidazolyl moiety in these more complex BPs with HA. As illustrated in Scheme 3, the protonated imidazole can interact with HA through the hydrogen bond N–H···O or N···H–O, which can optimally allow a bifurcated dual bonding arrangement. For optimal binding to HA, these hydrogen bonds require a N–H–O angle of larger than 125° and a N···O distance of approximately 3 Å.[8] This has been demonstrated by the optimal distance and angle of the N–H–O bond that can be formed with the alendronate $–NH_2$ and zoledronate distal heteroaromatic nitrogen, which can account for their higher binding affinity compared with that observed for other BPs. Therefore, it is inferred that imidazolyl-containing BPs **3a**–**e**, which can form any of these bonds, will have a higher affinity for bone mineral. However, although these BPs can theoretically orient properly for hydrogen bond formation, steric hindrance of different alkyl groups on the neighbouring position (N2) may interfere with these potential interactions, which may explain why **3b**–**e** have a lower binding affinity than **3a**.

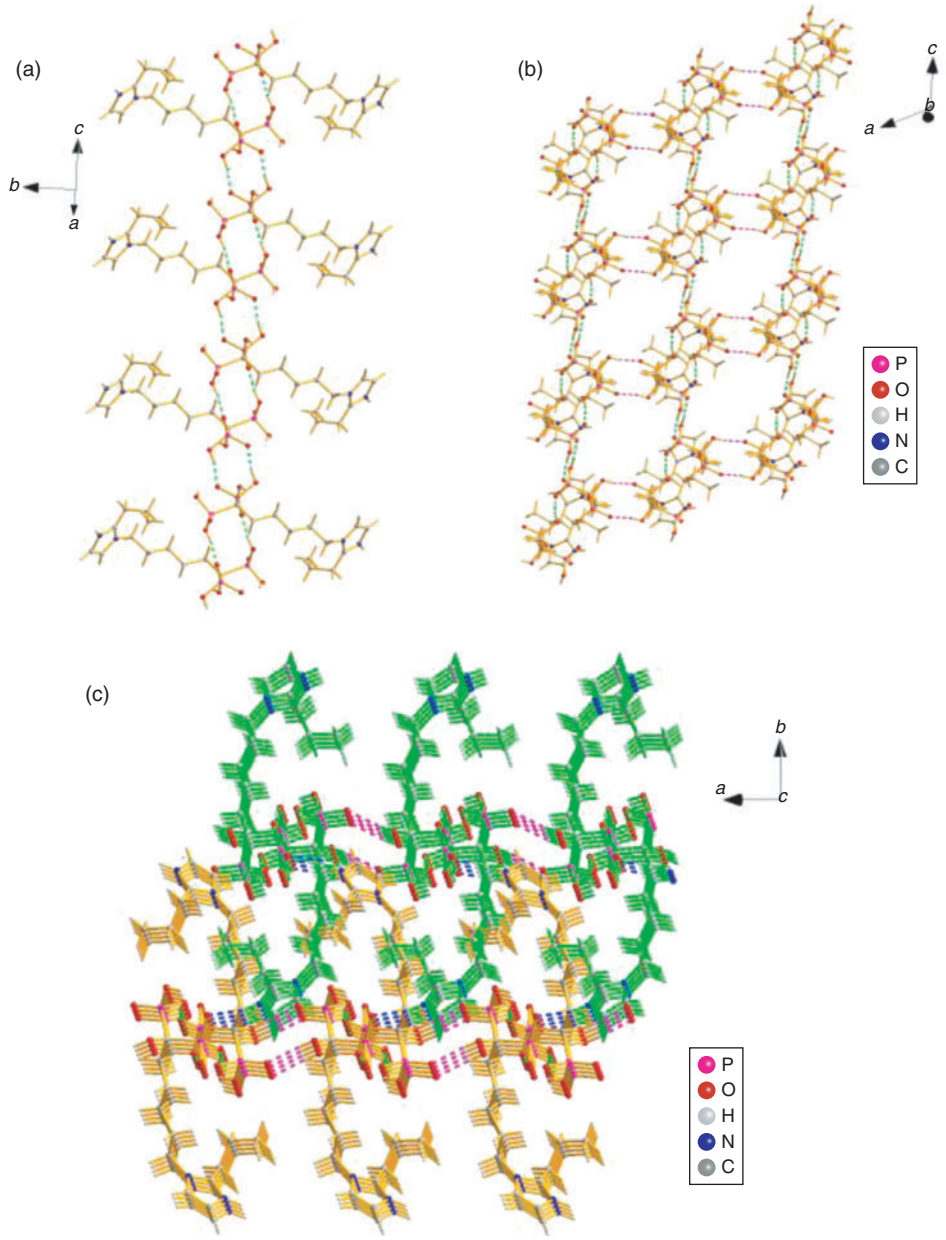

Fig. 6. Perspective view of the supramolecular network of compound **3d** formed by the hydrogen-bonding interactions from 1D (a), 2D (b), to 3D (c). Dashed lines represent hydrogen bonds.

Thus, the difference in the 3D configuration allowing the BPs to form different N–H–O bonds can explain the differences observed in the HA binding affinity, which may in turn have an influence over the pharmacological potency and clinical effects of BPs.[8] Since weak binding on HA may translate to lower potency that necessitates a higher dose, we postulate that a higher affinity of BPs **3a**–**e** for binding to HA may compensate for their low potency.

Conclusions

A series of novel imidazolyl-containing BPs were synthesised and identified by MS, IR spectroscopy, ^{1}H NMR spectroscopy, XRD, and HPLC. The synthetic route was attractive for its advantages including readily available reagents and high purity of final products under easy operating conditions. There exists many strong hydrogen bonds in the crystal structures among the phosphonate oxygens, hydroxy groups, and protonated nitrogen atoms as well as the lattice water molecules to form 3D supramolecular frameworks. The HPLC method was developed to determine the HA-binding affinity of BPs and it provides an accurate, precise, and robust method for quantitative analysis. Compound **3a** has the greatest affinity for HA with a maximal binding amount of 158.10 μmol g^{-1}, which is nearly 1.5–1.9 fold that of **3b**–**e**. These results provide a new example of how small differences in the BP structure can lead to significant changes in the bone binding affinity and capacity.

Supplementary Material

Standard concentration-area curves of BPs (Fig. 1S) and selected bond lengths and angles (Table S1) for compounds **3a**–**e** can be found on the Journal's website.

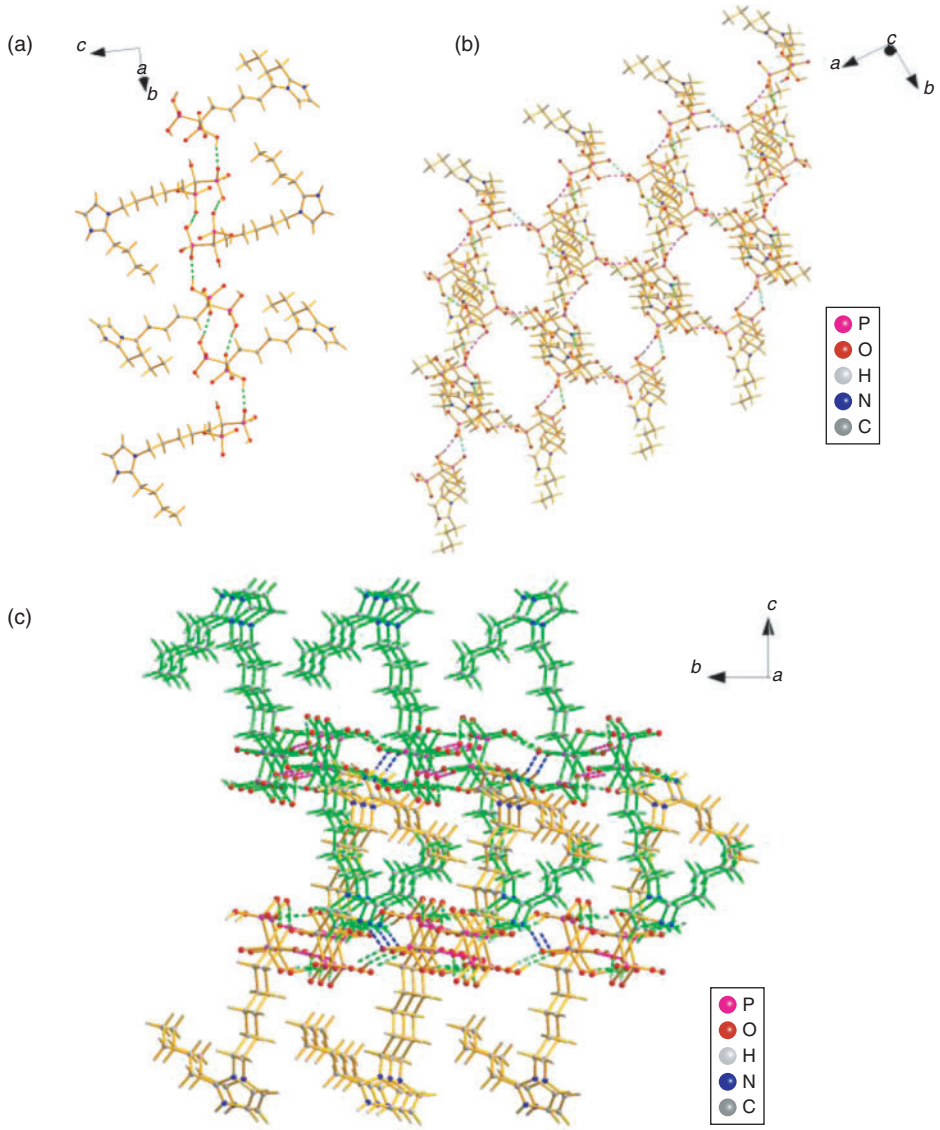

Fig. 7. Perspective view of the supramolecular network of compound **3e** formed by the hydrogen-bonding interactions from 1D (a), 2D (b), to 3D (c). Dashed lines represent hydrogen bonds.

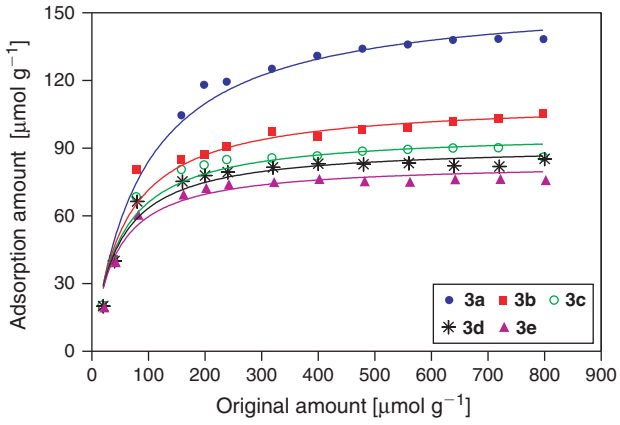

Fig. 8. Binding of compounds **3a–3e** to hydroxyapatite at 37°C after 48 h incubation.

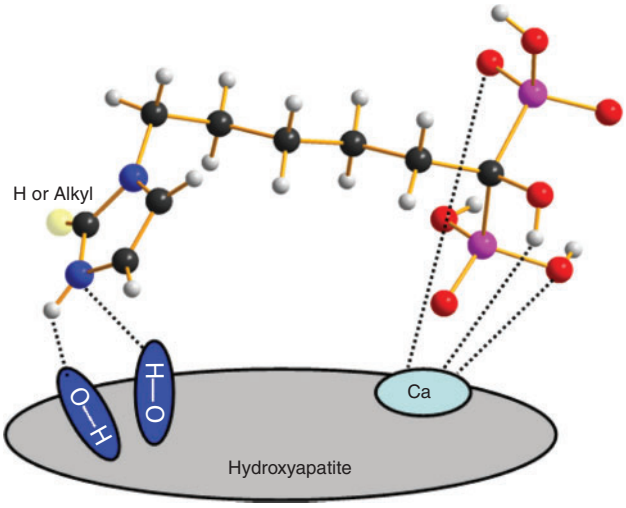

Scheme 3. Illustration of bisphosphonates **3a–e** binding to hydroxyapatite.

Acknowledgements

This work was financially supported by the National Natural Science Foundation of China (21001055 and 20801024), Natural Science Foundation of Jiangsu Province (BK2009077), and Key Medical Talent Project of Jiangsu Province (RC2011097).

References

[1] A. Jung, S. Bisaz, H. Fleisch, *Calcif. Tissue Res.* **1973**, *11*, 269. doi:10.1007/BF02547227

[2] G. A. Rodan, T. J. Martin, *Science* **2000**, *289*, 1508. doi:10.1126/SCIENCE.289.5484.1508

[3] (a) S. Vasireddy, A. Talwarkar, H. Miller, *Clin. Rheumatol.* **2003**, *22*, 376. doi:10.1007/S10067-003-0762-X
(b) R. E. Coleman, E. V. McCloskey, *Bone* **2011**, *49*, 71. doi:10.1016/J.BONE.2011.02.003
(c) A. Lipton, *ExpertOpin. Pharmaco* **2011**, *12*, 749.

[4] (a) E. Oldfield, *Acc. Chem. Res.* **2010**, *43*, 1216. doi:10.1021/AR100026V
(b) R. G. Russell, Z. Xia, J. E. Dunford, U. Oppermann, A. Kwaasi, P. A. Hulley, K. L. Kavanagh, J. T. Triffitt, M. W. Lundy, R. J. Phipps, B. L. Barnett, F. P. Coxon, M. J. Rogers, N. B. Watts, F. H. Ebetino, *N. Y. Ann. Acad. Sci.* **2007**, *1117*, 209. doi:10.1196/ANNALS.1402.089

[5] (a) D. M. Black, P. D. Delmas, R. Eastell, I. R. Reid, S. Boonen, J. A. Cauley, F. Cosman, P. Lakatos, P. C. Leung, Z. Man, C. Mautalen, P. Mesenbrink, H. Hu, J. Caminis, K. Tong, T. Rosario-Jansen, J. Krasnow, T. F. Hue, D. Sellmeyer, E.F. Eriksen, S. R. N. Cummings, *Engl. J. Med.* **2007**, *356*, 1809. doi:10.1056/NEJMOA067312
(b) G. Owens, R. Jackson, E. M. Lewiecki, *Am. J. Manag. Care.* **2007**, *13*, S290.
(c) R. C. Mühlbauer, F. Bauss, R. Schenk, M. Janner, E. Bosies, K. Strein, H. J. Fleisch, *Bone. Miner. Res.* **1991**, *6*, 1003. doi:10.1002/JBMR.5650060915

[6] O. L. M. Bijvoet, H. A. Fleisch, R. E. Canfield, R. G. G. Russell, *Biophosphonate on Bones* **1995** (Elsevier: Amsterdam).

[7] G. H. Nancollas, R. Tang, R. J. Phipps, Z. Henneman, S. Gulde, W. Wu, A. Mangood, R. G. G. Russell, F. Hebetino, *Bone* **2006**, *38*, 617. doi:10.1016/J.BONE.2005.05.003

[8] R. G. G. Russell, N. B. Watts, F. H. Ebetino, M. J. Rogers, *Osteoporos. Int.* **2008**, *19*, 733. doi:10.1007/S00198-007-0540-8

[9] J. E. Dunford, K. Thompson, F. P. Coxon, S. P. Luckman, F. M. Hahn, C. D. Poulter, F. H. Ebetino, M. J. J. Rogers, *Pharmacol. Exp. Ther.* **2001**, *296*, 235.

[10] M. R. Smith, *Urol. Oncol: Semin. Orig. Investig.* **2008**, *26*, 420. doi:10.1016/J.UROLONC.2007.11.004

[11] J. A. Kanis, B. J. Gertz, F. Singer, S. Ortolani, *Osteoporos. Int.* **1995**, *5*, 1. doi:10.1007/BF01623652

[12] (a) L. Widler, K. A. Jaeggi, M. Glatt, K. Müller, R. Bachmann, M. Bisping, A. R. Born, R. Cortesi, G. Guiglia, H. H. Jeker, R. Klein, U. Ramseier, J. Schmid, G. Schreiber, Y. Seltenmeyer, J. R. Green, *J. Med. Chem.* **2002**, *45*, 3721. doi:10.1021/JM020819I
(b) C. M. Szabo, M. B. Martin, E. Oldfield, *J. Med. Chem.* **2002**, *45*, 2894. doi:10.1021/JM010279+
(c) Y. Zhang, A. Leon, Y. Song, D. Studer, C. Haase, L. A. Koscielski, E. Oldfield, *J. Med. Chem.* **2006**, *49*, 5804. doi:10.1021/JM060280E
(d) J. H. Mao, S. Mukherjee, Y. Zhang, R. Cao, M. S. Ohn, Y. C. Song, Y. H Zhang, A. M. Gary, Y. G. Gao, D. Mukkamala, P. H. Michael, E. Oldfield, *J. Am. Chem. Soc.* **2006**, *128*, 14485. doi:10.1021/JA061737C
(e) R. T. M. Rosales, C. Finucane, S. J. Mather, P. J. Blower, *Chem. Commun.* **2009**, 4847. doi:10.1039/B908652H
(f) F. H. Ebetino, A. M. Hogan, S. Sun, M. K. Tsoumpra, X. Duan, J. T. Triffitt, A. A. Kwaasi, J. E. Dunford, B. L. Barnett, U. Oppermann, M. W. Lundy, A. Boyde, B. A. Kashemirov, C. E. McKenna, R. G. Russell, *Bone* **2011**, *49*, 20. doi:10.1016/J.BONE.2011.03.774

[13] (a) X. H. Guo, S. N. Luo, H. Y. Wang, L. Zhou, M. H. Xie, W. Z. Ye, M. Yang, Y. Wang, *Nucl. Sci. Technol.* **2006**, *17*, 285. doi:10.1016/S1001-8042(06)60053-5
(b) J. G. Lin, S. N. Luo, C. Q. Chen, L. Qiu, Y. Wang, W. Cheng, W. Z. Ye, Y. M. Xia, *Appl. Radiat. Isot.* **2010**, *68*, 1616. doi:10.1016/J.APRADISO.2010.03.009
(c) J. G. Lin, L. Qiu, W. Cheng, S. N. Luo, W. Z. Ye, *Nucl. Med. Biol.* **2011**, *38*, 619. doi:10.1016/J.NUCMEDBIO.2010.12.005
(d) J. Lin, L. Qiu, W. Cheng, S. N. Luo, L. Xue, S. Zhang, *Appl. Radiat. Isot.* **2012**, *70*, 848. doi:10.1016/J.APRADISO.2011.12.019
(e) L. Qiu, J. G. Lin, S. N. Luo, Y. Wang, W. Cheng, S. Zhang, *Radiochim. Acta* **2012**, *100*, 463. doi:10.1524/RACT.2012.1934

[14] G. M. Sheldrick, *SHELXS-97*, *Program for X-Ray Crystal Structure Solution* **1997** (University of Götingen: Götingen, Germany).

[15] G. M. Sheldrick, *SHELXL-97*, *Program for X-Ray Crystal Structure Refinement* **1997** (University of Götingen: Götingen, Germany).

[16] (a) A. Cabeza, X. Ouyang, C. V. K. Sharma, M. A. G. Aranda, S. Bruque, A. Clearfield, *Inorg. Chem.* **2002**, *41*, 2325. doi:10.1021/IC0110373
(b) H. S. Martinez-Tapia, A. Cabeza, S. Bruque, P. Pertierra, S. Garcia-Granda, M. A. G. Aranda, *J. Solid State Chem.* **2000**, *151*, 122. doi:10.1006/JSSC.2000.8634

[17] B. Hemmateenejad, M. Shamsipur, A. Safavi, H. Sharghi, A. A. Amiri, *Talanta* **2008**, *77*, 351. doi:10.1016/J.TALANTA.2008.06.044

[18] (a) K. Ravikumar, B. Sridhar, *Acta Crystallogr. C* **2010**, *66*, o97. doi:10.1107/S0108270110000958
(b) S. J. Li, W. D. Song, S. H. Li, J. J. Dong, J. B. Yan, *Acta Crystallogr.* **2010**, *E66*, m1094.

[19] R. Ruscica, M. Bianchi, M. Quintero, A. Martinez, D. R. Vega, *J. Pharm. Sci.* **2010**, *99*, 4962. doi:10.1002/JPS.22223

[20] (a) D. R. Vega, D. Fernández, J. A. Ellena, *Acta Crystallogr. C* **2002**, *58*, m77. doi:10.1107/S0108270101019655
(b) D. Fernández, D. R. Vega, *Acta Crystallogr. C* **2003**, *59*, o228. doi:10.1107/S0108270103006085
(c) W. L. Gossman, S. R. Wilson, E. Oldfield, *Acta Crystallogr. C.* **2003**, *59*, m33. doi:10.1107/S0108270102021996
(d) S. Wu, S. Chen, M. Li, J. Xiang, Y. Xiao, L. Yuan, *CrystEngComm* **2007**, *9*, 907. doi:10.1039/B706485C

[21] F. H. Allen, O. Kennard, D. G. Watson, L. Brammer, A. G. Orpen, R. Taylor, *J. Chem. Soc. Perkin Trans. 2* **1987**, *II*, S1.

[22] (a) A. Bondi, *J. Phys. Chem.* **1964**, *68*, 441. doi:10.1021/J100785A001
(b) Y. Wang, T. Okamura, W. Y. Sun, N. Ueyama, *Cryst. Growth Des.* **2008**, *8*, 802. doi:10.1021/CG701242Z

[23] K. McLeod, G. I. Anderson, N. K. Dutta, R. S. C. Smart, N. H. Voelcker, R. Sekel, S. Kumar, *J. Biomed. Mater. Res. A* **2006**, *79A*, 271. doi:10.1002/JBM.A.30792

[24] W. Jahnke, C. Henry, *ChemMedChem* **2010**, *5*, 770. doi:10.1002/CMDC.201000016

[25] V. Hengst, C. Oussoren, T. Kissel, G. Storm, *Int. J. Pharm.* **2007**, *331*, 224. doi:10.1016/J.IJPHARM.2006.11.024

[26] M. A. Lawson, Z. Xia, B. L. Barnett, J. T. Triffitt, R. J. Phipps, J. E. Dunford, R. M. Locklin, F. H. Ebetino, R. G. G. Russell, *J. Biomed. Mater. Res. B.* **2010**, *92*, 149.

[27] F. H. Ebetino, P. Emmerling, B. Barnett, G. H. Nancollas, *J. Bone Miner. Res.* **2004**, *19*, S157.

[28] Z. J. Henneman, G. H. Nancollas, F. H. Ebetino, R. J. Phipps, R. G. G. Russell, *J. Biomed. Mater. Res. A* **2008**, *85A*, 993. doi:10.1002/JBM.A.31599